nature photonics

LETTERS

https://doi.org/10.1038/s41566-018-0281-6

Corrected: Author Correction

Microwave plasmonic mixer in a transparent fibre–wireless link

Y. Salamin[1*], B. Baeuerle[1], W. Heni[1], F. C. Abrecht[1], A. Josten[1], Y. Fedoryshyn[1], C. Haffner[1], R. Bonjour[1], T. Watanabe[1], M. Burla[1], D. L. Elder[2], L. R. Dalton[2] and J. Leuthold[1*]

To cope with the high bandwidth requirements of wireless applications[1], carrier frequencies are shifting towards the millimetre-wave and terahertz bands[2–5]. Conversely, data is normally transported to remote wireless antennas by optical fibres. Therefore, full transparency and flexibility to switch between optical and wireless domains would be desirable[6,7]. Here, we demonstrate a direct wireless-to-optical receiver in a transparent optical link. We successfully transmit 20 and 10 Gbit s^{-1} over wireless distances of 1 and 5 m, respectively, at a carrier frequency of 60 GHz. Key to the breakthrough is a plasmonic mixer directly mapping the wireless information onto optical signals. The plasmonic scheme with its subwavelength feature and pronounced field confinement provides a built-in field enhancement of up to 90,000 over the incident field in an ultra-compact and complementary metal-oxide–semiconductor compatible structure. The plasmonic mixer is not limited by electronic speed and thus compatible with future terahertz technologies.

High-capacity millimetre-wave (MMW) and terahertz (THz) links require efficient transmitters and receivers. In this context, photonics—or microwave photonics—has emerged as a successful approach to overcome electronic-related speed limitations[2,3,7]. And indeed, the community has come up with most efficient optical-to-wireless transmitters that work reliably up to 400 GHz (refs [8–10]). Furthermore, fully integrated transmitters have been demonstrated[11–13]. However, the reception of wireless signals and the direct upconversion to an optical signal has been, and remains, a challenge.

Until now, wireless-to-optical receiver systems have mainly relied on high-speed electronics[14]. Usually, the signal is received by an antenna, pre-amplified, and mixed down to the baseband or to an intermediary frequency with an electronic mixer. After an additional amplification stage, the signal is converted to the optical domain by means of an electro-optic modulator[7]. Therefore, a simple solution that would allow a direct wireless-to-optical conversion (omitting electronics) is of great interest—particularly if realized on a low-cost platform such as silicon[15]. A possible application scenario in access networks[6] is depicted in Fig. 1.

Recently, a wireless-to-optical conversion without radiofrequency down-mixing was demonstrated over a distance of 4 m (ref. [16]). Ten gigabaud (GBd) 16-quadrature amplitude modulation (QAM) signals from two external antennas were separately amplified and then converted back to the optical domain by a dual-polarization modulator. This approach is interesting, yet, an electro-optic device capable of directly converting the wireless signal to the optical domain would strongly reduce the complexity, cost and bulkiness of MMW and THz receivers. Most importantly, an electro-optical approach would not require any high-frequency front-end electronics, in which the wireless carrier frequency would ultimately be limited by the electronic speed. Surely, several direct wireless-to-optical converters with an antenna directly combined with an optical modulator have been demonstrated[17–20]. For instance, successful photonics-based electro-optic conversion of 60 GHz and 14 GHz sinusoidal carriers have been demonstrated over distances of 25 cm and 40 cm, respectively. These demonstrations used respectively nonlinear optical materials such as lithium niobate[17] or organic polymer[20]. Recently, a direct radiofrequency-photonic receiver at 36 GHz with a 1 MBd 64-QAM signal for a 23 cm link was demonstrated[19]. While these are interesting approaches, it is clear that the current approaches either suffer from electro-optical bandwidth limitations that makes a transition to higher carrier frequencies difficult or that they require a considerably more sensitive reception that would allow a higher modulation. In parallel, plasmonics[21] has emerged as a field that offers almost unlimited bandwidth[22] and impressive modulation depths at very low electrical fields[23] owing to their subwavelength confinement capabilities[24]. These unique features make plasmonic electro-optic phase modulators an ideal candidate for the direct wireless-to-optical conversion up to THz frequencies[18,25]. Recently, it has been shown that by combining a plasmonic electro-optic phase modulator[26] with a dipole antenna, a 60 GHz signal can be mapped to the optical domain with high conversion efficiency[27].

Here, we demonstrate a direct wireless-to-optical conversion with a plasmonic phase modulator directly integrated with a resonant four-leaf-clover (4LC) antenna. The performance of the converter is shown in a 20 Gbit s^{-1} and 10 Gbit s^{-1} line-rate experiment at a 60 GHz carrier frequency over the free-space distances of 1 m and 5 m, respectively. No radiofrequency front-end electronics were required in the wireless-to-optical receiver because the scheme offers an inherent built-in plasmonic field enhancement up to 90,000. The complete electro-optic device requires only 0.315 mm^2 of footprint and is scalable from GHz to THz, and the fabrication is compatible with standard silicon technologies. Such a device not only can pave the path for new applications, but also may give way to new array systems such as needed for high-data-rate beam steering[7].

The device, shown in Fig. 2a, consists of a MMW antenna and a plasmonic phase modulator combined in one single metallic structure. Light guided by silicon (Si) waveguides is converted to and from surface plasmon polaritons (SPPs) by photonic-plasmonic converters[26]. The SPPs propagate along the plasmonic modulator formed by a horizontally aligned metal–insulator–metal (MIM) slot waveguide[28] filled with a nonlinear organic material[29]. When an

[1]Institute of Electromagnetic Fields (IEF), ETH Zurich, Zurich, Switzerland. [2]Department of Chemistry, University of Washington, Seattle, WA, USA.
*e-mail: yannick.salamin@ief.ee.ethz.ch; juerg.leuthold@ief.ee.ethz.ch

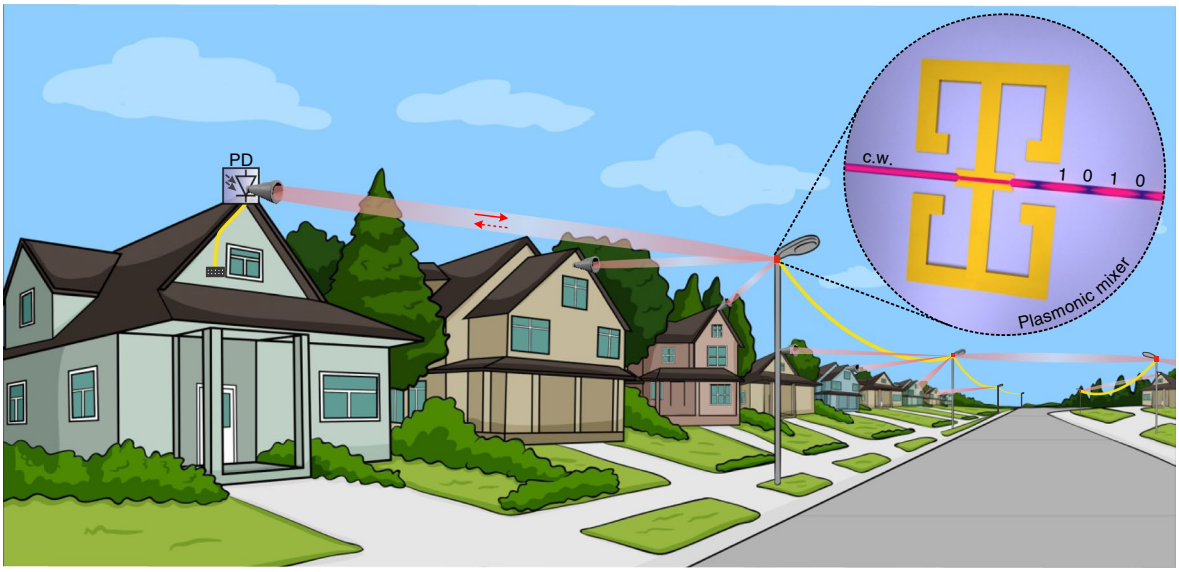

Fig. 1 | Prospective application scenario for a point-to-point high-capacity fibre–wireless link. Deploying the fibre-to-the-home can be costly. One possible scenario to reduce the cost, while still providing high-capacity connectivity for the end user, is to use virtual fibres (red beams) for the last few metres. Here, optical fibres (yellow lines) are deployed to the residential area either underground or aboveground using existing cable platforms. Lamp posts located close to the houses could host optical-to-wireless converters for the downstream data (red dashed arrow) and wireless-to-optical converters (plasmonic mixer) for the upstream data (red arrow). A direct converter could very simply and cost efficiently map the wireless signal onto a common laser signal, which then can be routed back to the central office. PD, photodiode; c.w., continuous wave.

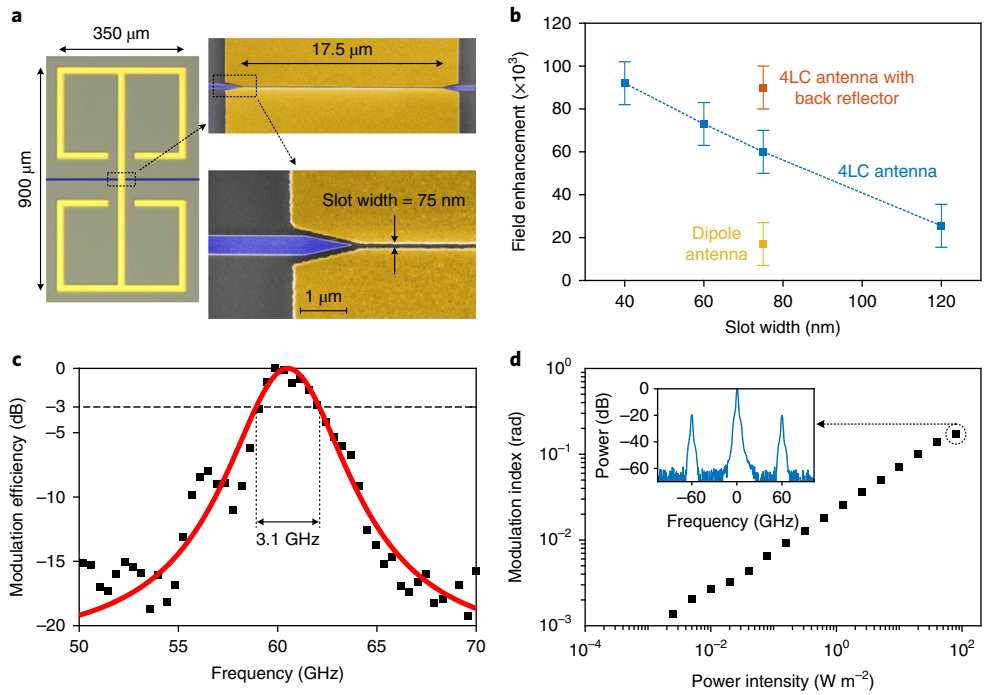

Fig. 2 | Device structure and performance. a, Left: top view of an optical microscope image of the 4LC antenna with the integrated plasmonic phase modulator. Right: Zoomed-in scanning electron microscope colourized images of the phase-modulator section (top) and detail view of the photonic-to-plasmonic converter (bottom). **b**, Field enhancement provided by the structure as a function of the slot width. The blue dashed line is a linear interpolation intended as a visual guide. Error bars indicate the ±10% error margin. **c**, Electro-optical bandwidth of the plasmonic mixer. The black squares are the measured data and the overlapping red line is a fit with a Lorentzian function. The horizontal dashed line shows the 3 dB electro-optical bandwidth. **d**, Modulation index as a function of the power intensity at the plasmonic mixer. The measurement is based on a 5 m link. The inset shows the normalized electro-optical response of the plasmonic mixer.

incident MMW field couples to the resonant antenna, charge carriers oscillate with the incident field producing an electric field across the MIM slot. As the metallic antenna arms are used to form the plasmonic MIM slot, all the voltage drop occurs across the nonlinear material. Owing to the Pockels effect, the refractive index of the nonlinear material in the slot changes linearly with the incident

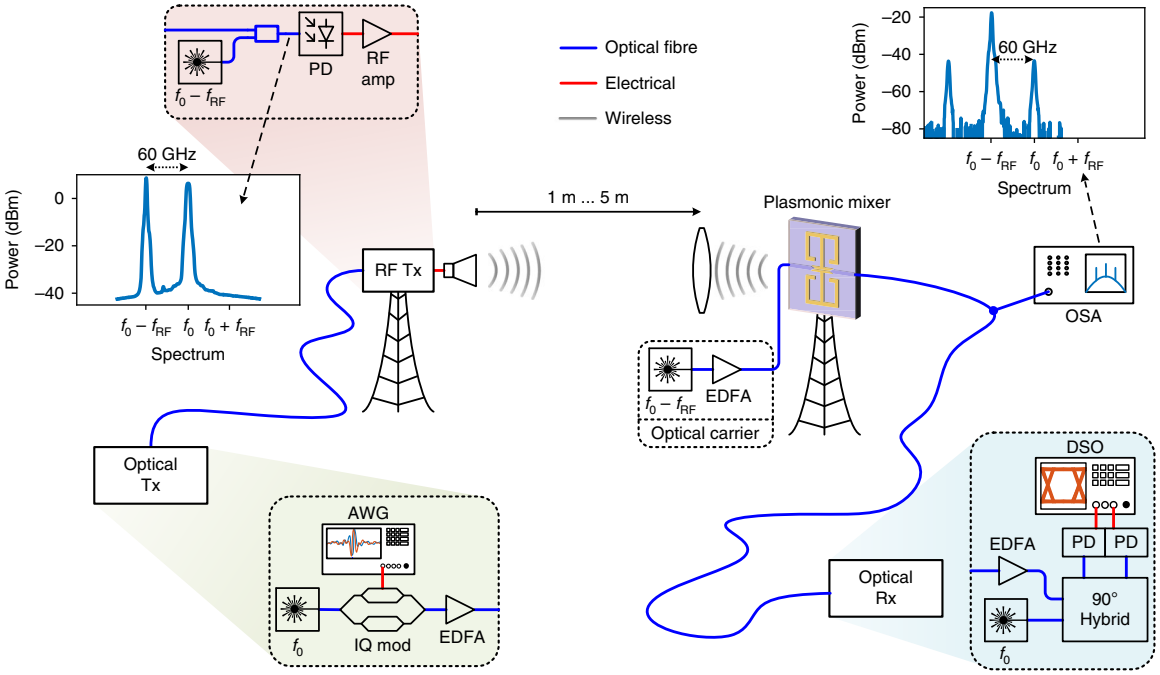

Fig. 3 | Fibre-to-wireless and wireless-to-fibre link experiment. First the optical signal is generated by encoding a QPSK signal with a random bit sequence of length 40,960 onto a 1,550 nm optical carrier (f_0). The optical signal (10 dBm) is subsequently combined with a reference laser ($f_0 - f_{RF}$) detuned by the wireless carrier frequency (f_{RF}) of 60 GHz and fed into a high-speed photodetector. The resulting MMW signal is amplified and emitted to the far-field by a high-gain MMW antenna. The wireless signal is focused by means of a high-density polyethylene lens onto the plasmonic mixer and converted back to the optical domain. The optical signal is decoded in a coherent receiver system consisting of a 90° hybrid mixer and photodetectors. RF, radiofrequency; Tx, transmitter; Rx, receiver; IQ mod, IQ modulator; AWG, arbitrary waveform generator; EDFA, erbium-doped fibre amplifier; PD, photodiode; RF amp, radiofrequency amplifier; OSA, optical spectrum analyser; DSO, real-time digital storage oscilloscope.

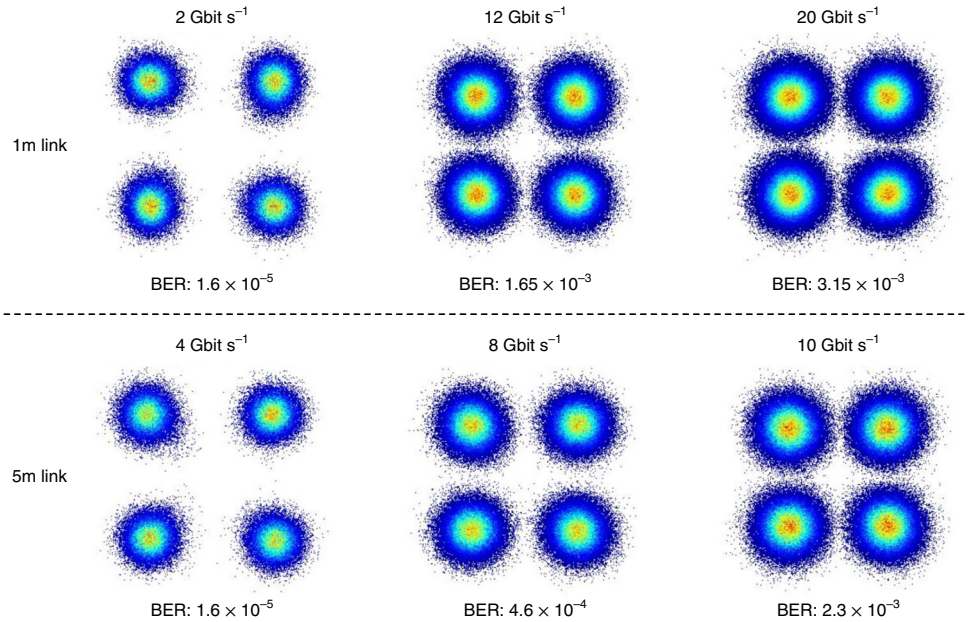

Fig. 4 | Experimental results. Fibre–wireless transmission experiment results for 1 m and 5 m wireless link. Constellation diagrams at 2, 12 and 20 Gbit s^{-1} are shown for a wireless distance of 1 m. For the 5 m wireless link experiment, the constellation diagram at 2, 8 and 10 Gbit s^{-1} are shown.

MMW field strength (see Methods). This way, a wireless signal can directly modulate the phase of a SPP propagating along the slot.

The proposed structure can efficiently convert wireless signals to the optical domain for mainly three reasons. First, the nanoscale slot provided by plasmonics gives rise to a strong field enhancement due to the inverse dependency of the field with the slot width. Second, the resulting electric field in the slot overlaps almost perfectly with the optical field propagating along the MIM slot waveguide leading

to a strong nonlinear interaction (see Supplementary section 1). Third, the resonant nature of the 4LC antenna further enhances the electric field in the slot and is maximized by fulfilling the full-wave resonance condition[30] (see Supplementary section 2). In this respect, a trade-off between achievable field enhancement and the available bandwidth limits the design. Even though the wavelength of the 60 GHz carrier is 5 mm in free space, owing to the high-k silicon substrate, the dimensions of the antenna can be below mm^2, which is a benefit for integration.

Devices were fabricated on a silicon-on-insulator (SOI) wafer (Fig. 2a and Methods). The electro-optic conversion efficiency of the device was tested first. From the measured modulation depth (see Methods), one can calculate the field enhancement achieved by the structure[27]. As expected, a slot-width dependency is observed (Fig. 2b, blue squares). Although the highest field enhancement is achieved for narrow slots, the insertion losses and poling efficiency play a role in the overall conversion performance and have slot-width dependency as well[31]. The optimal slot width is found to be around 75 nm. A field enhancement of up to 60,000 was found for the device with the 75-nm-wide plasmonic slot (Fig. 2b, blue squares). The device with a back reflector has an increased field enhancement of 90,000 (Fig. 2b, red square). Comparing the field enhancement of a simple dipole antenna structure (Fig. 2b, yellow square) with the 4LC antenna, a clear increase in the efficiency can be observed for the 4LC structures. The bandwidth around the 60 GHz carrier was measured and found to be 3.1 GHz (Fig. 2c), close to the expected value of the designed resonant antenna. This corresponds to a relative bandwidth of 5%. The antenna with back reflector had an increased relative bandwidth of 10%. This is slightly less than the relative bandwidth of 12%, for example, available in ref [16]. However, the relative bandwidth in our approach can be adapted by choosing another resonant structure. So, for instance, a dipole antenna can provide relative bandwidths beyond 25% (refs [27,32]). Figure 2d shows the modulation depth achievable as a function of the power intensity at the receiver. A linear dependency is observed, and strong modulation can be achieved even with reasonable transmitted power. A modulation index of 0.2 rad is easily achieved for a wireless distance of 5 m. Such a modulation index corresponds to an equivalent applied voltage of 0.8 V, and is sufficient for high-data-rate modulation[23].

To test the device in a last-metre scenario as depicted in Fig. 1, a transparent fibre–wireless–fibre link was built, as shown in Fig. 3 (see Supplementary section 3). First the electrical data consisting of a quadrature phase shift keying (QPSK) signal with a random bit sequence of length 40,960 is encoded on an optical carrier (f_0) by means of an in-phase and quadrature (IQ) modulator (optical transmitter). Ultimately, the goal is to transmit multiples of 10 Gbit s^{-1}—which is a standard in datacom and fibre-to-the-home. Subsequently, the optical signal is converted to a MMW wireless signal (radiofrequency transmitter) by a heterodyne approach (see Methods). The wireless signal (f_{RF}) is focused on the passive plasmonic mixer by means of a high-density polyethylene lens and converted back on an optical carrier ($f_0 - f_{RF}$). Finally, the electrical signal is recovered in a coherent optical receiver. The wireless link between the transmitter and receiver was tested in a 1 m and 5 m scenario with two different 4LC devices with and without back reflector, respectively.

The results of the fibre–wireless–fibre data experiment are shown in Fig. 4. Line rates of 2 Gbit s^{-1} and up to 20 Gbit s^{-1} were achieved for the 1 m link with bit-error ratios (BERs) of 1.6×10^{-5} to 3.1×10^{-3}, and line rates of 4 Gbit s^{-1} and up to 10 Gbit s^{-1} for a 5 m link with BERs of 1.6×10^{-5} to 2.3×10^{-3}. Note that no electronics were used in the passive wireless-to-optical receiver. Errors in signals with BERs below the hard-decision forward error correction limit[33] of 4.5×10^{-3} can be corrected with a small overhead of 7%.

To assess the limits and opportunities of the proposed plasmonic mixer technology one can resort to the bandwidth-distance product as a figure of merit. The bandwidth and distance are defined respectively by the 3 dB electro-optical bandwidth times the distance at which the achievable BER stays below the hard-decision forward error correction limit. With this figure of merit, we obtain for the first experiment (1 m link) a 6 GHz m bandwidth-distance product and in the second experiment (5 m link) a 15 GHz m bandwidth-distance product. These numbers need to be taken with care though as they do not show what is really possible. For instance, the transmitter and receiver antenna link gain in our setup account for a 56 dBi gain, whereas in literature schemes more than 86 dBi is frequently used[4,8,34]. This would leave a margin of more than 30 dB of link gain if needed. Also, in our first chip generations, we report fibre-to-fibre losses of 44 and 34 dB for the two generations of devices. These optical losses are high. Yet, by resorting to fibre-to-chip schemes offered by foundries[35] and by exploiting the most recent resonant plasmonic structures,[36] the overall chip losses can be as low as 8 dB (see Methods). There is thus a 26 dB optical link gain—corresponding to a 52 dB electrical gain that one can still take advantage of. Lastly, the scheme is scalable to higher carrier frequencies, such as 300 GHz. This is possible as the frequency response of the plasmonic modulator is flat up to 325 GHz (refs [22,25,37]). When working with three high-carrier-frequency bands[38] one could envision a capacity beyond 180 Gbit s^{-1} (see Methods). To sum up, the discussion shows that the suggested scheme has ample margin and a bandwidth-distance product of as much as, for example, 9 THz m is surely doable. This could, for instance, be achieved by the aforementioned 180 Gbit s^{-1} QPSK link if transmitted over a distance of 100 m.

Other opportunities will emerge with the rise of phased-array beam-steering technologies[39]. The microwave plasmonic scheme offers a unique advantage as it scales well both in footprint and speed. The scaling is due to the fact that the receiving antenna is extremely compact and may operate up to the highest carrier frequencies.

In conclusion, we have demonstrated a transparent fibre–wireless link with an entirely integrated direct wireless-to-optical receiver. Key to this was a novel plasmonic mixer that can directly convert a wireless 60 GHz signal to the optical domain. Line rates of 20 Gbit s^{-1} were successfully transmitted across a 1 m free-space radiofrequency link and up to 5 m at 10 Gbit s^{-1}. The receiver is as compact as 0.315 mm^2, which makes it potentially attractive for use in next-generation wireless and phased-array systems.

Received: 13 March 2018; Accepted: 21 September 2018;
Published online: 29 October 2018

References

1. Waterhouse, R. & Novak, D. Realizing 5G: microwave photonics for 5G mobile wireless systems. *IEEE Microw. Mag.* **16**, 84–92 (2015).
2. Capmany, J. & Novak, D. Microwave photonics combines two worlds. *Nat. Photon.* **1**, 319–330 (2007).
3. Yao, J. Microwave photonics. *J. Lightw. Technol.* **27**, 314–335 (2009).
4. Nagatsuma, T., Ducournau, G. & Renaud, C. C. Advances in terahertz communications accelerated by photonics. *Nat. Photon.* **10**, 371–379 (2016).
5. Seeds, A. J., Shams, H., Fice, M. J. & Renaud, C. C. Terahertz photonics for wireless communications. *J. Lightw. Technol.* **33**, 579–587 (2015).
6. Lim, C. et al. Fiber-wireless networks and subsystem technologies. *J. Lightw. Technol.* **28**, 390–405 (2010).
7. Shams, H. & Seeds, A. Photonics, fiber and THz wireless communication. *Opt. Photon. News* **28**, 24–31 (2017).
8. Koenig, S. et al. Wireless sub-THz communication system with high data rate. *Nat. Photon.* **7**, 977–981 (2013).
9. Ducournau, G. et al. Ultrawide-bandwidth single-channel 0.4-THz wireless link combining broadband quasi-optic photomixer and coherent detection. *IEEE Trans. Terahertz Sci. Technol.* **4**, 328–337 (2014).
10. Yu, X. et al. 400-GHz wireless transmission of 60-Gb/s Nyquist-QPSK signals using UTC-PD and heterodyne mixer. *IEEE Trans. Terahertz Sci. Technol.* **6**, 765–770 (2016).

11. Ito, H., Nakajima, F., Furuta, T. & Ishibashi, T. Continuous THz-wave generation using antenna-integrated uni-travelling-carrier photodiodes. *Semicond. Sci. Technol.* **20**, S191 (2005).
12. Yardimci, N. T., Cakmakyapan, S., Hemmati, S. & Jarrahi, M. A high-power broadband terahertz source enabled by three-dimensional light confinement in a plasmonic nanocavity. *Sci. Rep.* **7**, 4166 (2017).
13. Renaud, C. C. et al. Antenna integrated THz uni-traveling carrier photodiodes. *IEEE J. Sel. Top. Quantum Electron.* **24**, 1–11 (2018).
14. Li, X., Yu, J., Xiao, J. & Xu, Y. Fiber-wireless-fiber link for 128-Gb/s PDM-16QAM signal transmission at *W*-band. *IEEE Photon. Technol. Lett.* **26**, 1948–1951 (2014).
15. Marpaung, D. et al. Integrated microwave photonics. *Laser Photon. Rev.* **7**, 506–538 (2013).
16. Yang, C., Li, X., Xiao, J., Chi, N. & Yu, J. Fiber-wireless integration for 80 Gbps polarization division multiplexing—16QAM signal transmission at *W*-band without RF down conversion. *Microw. Opt. Technol. Lett* **57**, 9–13 (2015).
17. Wijayanto, Y. N., Murata, H. & Okamura, Y. Electrooptic millimeter-wave-lightwave signal converters suspended to gap-embedded patch antennas on low-*k* dielectric materials. *IEEE J. Sel. Top. Quantum Electron.* **19**, 33–41 (2013).
18. Zhang, X. et al. Integrated photonic electromagnetic field sensor based on broadband bowtie antenna coupled silicon organic hybrid modulator. *J. Lightw. Technol.* **32**, 3774–3784 (2014).
19. Park, D. et al. RF photonic downconversion of vector modulated signals based on a millimeter-wave coupled electrooptic nonlinear polymer phase-modulator. *Opt. Express* **25**, 29885–29895 (2017).
20. Chung, C. J. et al. Silicon-based hybrid integrated photonic chip for Ku band electromagnetic wave sensing. *J. Lightw. Technol.* **36**, 1568–1575 (2018).
21. Brongersma, M. L. & Shalaev, V. M. The case for plasmonics. *Science* **328**, 440–441 (2010).
22. Hoessbacher, C. et al. Plasmonic modulator with >170 GHz bandwidth demonstrated at 100 GBd NRZ. *Opt. Express* **25**, 1762–1768 (2017).
23. Baeuerle, B. et al. Driver-less sub $1V_{PP}$ operation of a plasmonic-organic hybrid modulator at 100 GBd NRZ. in *Optical Fiber Communication Conference* M2I.1 (Optical Society of America, 2018).
24. Gramotnev, D. K. & Bozhevolnyi, S. I. Plasmonics beyond the diffraction limit. *Nat. Photon.* **4**, 83–91 (2010).
25. Benea-Chelmus, I.-C. et al. Three-dimensional phase modulator at telecom wavelength acting as a terahertz detector with an electro-optic bandwidth of 1.25 terahertz. *ACS Photon.* **5**, 1398–1403 (2018).
26. Haffner, C. et al. Plasmonic organic hybrid modulators—scaling highest speed photonics to the microscale. *Proc. IEEE* **104**, 2362–2379 (2016).
27. Salamin, Y. et al. Direct conversion of free space millimeter waves to optical domain by plasmonic modulator antenna. *Nano. Lett.* **15**, 8342–8346 (2015).
28. Pile, D. F. P. et al. Two-dimensionally localized modes of a nanoscale gap plasmon waveguide. *Appl. Phys. Lett.* **87**, 261114 (2005).
29. Elder, D. L. et al. Effect of rigid bridge-protection units, quadrupolar interactions, and blending in organic electro-optic chromophores. *Chem. Mater.* **29**, 6457–6471 (2017).
30. Woo, I., Nguyen, T. K., Han, H., Lim, H. & Park, I. Four-leaf-clover-shaped antenna for a THz photomixer. *Opt. Express* **18**, 18532–18542 (2010).
31. Heni, W. et al. Nonlinearities of organic electro-optic materials in nanoscale slots and implications for the optimum modulator design. *Opt. Express* **25**, 2627–2653 (2017).
32. Mokhtari-Koushyar, F. et al. Wideband multi-arm bowtie antenna for millimeter wave electro-optic sensors and receivers. *J. Lightw. Technol.* **36**, 3418–3426 (2018).
33. Chang, F., Onohara, K. & Mizuochi, T. Forward error correction for 100 G transport networks. *IEEE Commun. Mag.* **48**, S48–S55 (2010).
34. Kallfass, I. et al. 64 Gbit/s transmission over 850 m fixed wireless link at 240 GHz carrier frequency. *J. Infrared Millim. Terahertz Waves* **36**, 221–233 (2015).
35. Vermeulen, D. et al. High-efficiency fiber-to-chip grating couplers realized using an advanced CMOS-compatible silicon-on-insulator platform. *Opt. Express* **18**, 18278–18283 (2010).
36. Haffner, C. et al. Low-loss plasmon-assisted electro-optic modulator. *Nature* **556**, 483–486 (2018).
37. Ummethala, S. et al. Terahertz-to-optical conversion using a plasmonic modulator. in *Conference on Lasers and Electro-Optics* STu3D.4 (Optical Society of America, 2018).
38. Jia, S. et al. 120 Gb/s multi-channel THz wireless transmission and THz receiver performance analysis. *IEEE Photon. Technol. Lett.* **29**, 310–313 (2017).
39. Sun, J., Timurdogan, E., Yaacobi, A., Hosseini, E. S. & Watts, M. R. Large-scale nanophotonic phased array. *Nature* **493**, 195–199 (2013).

Acknowledgements

This work was carried out partially at the Binnig and Rohrer Nanotechnology Center (BRNC) and in the FIRST lab cleanroom facility at ETH Zurich. We are grateful to H. R. Benedickter and U. Drechsler for the help in the measurement and fabrication, respectively. The European Union project ERC PLASILOR (670478) and PLASMOfab (688166) are acknowledged for partial funding of the work. The US National Science Foundation (DMR-1303080) and the Air Force Office of Scientific Research (FA9550-15-1-0319). The ETH Postdoctoral Fellowship (16-2-FEL-51). M.B. acknowledges the SNSF Ambizione grant (173996).

Author contributions

Y.S conceived the concept, designed and fabricated the device, designed and performed the experiments and analysed the data. B.B., F.C.A. and A.J. performed the data experiment and data analysis. W.H. fabricated the device, developed the poling process and contributed to the measurements. Y.F. fabricated the device. C.H. contributed to the design of the device and experiment. R.B. and M.B. contributed to the design of the experiment. T.W contributed to the design of the device. D.L.E. and L.R.D. developed and synthesized the HD-BB-OH/YLD124 nonlinear material. J.L. conceived the concept and supervised the project. All authors have contributed to the writing of the manuscript.

Competing interests

The authors declare no competing interests.

Additional information

Supplementary information is available for this paper at https://doi.org/10.1038/s41566-018-0281-6.

Correspondence and requests for materials should be addressed to Y.S. or J.L.

Methods

Plasmonic phase modulator. The plasmonic phase modulator is based on a MIM slot (see Supplementary Fig. 1a) guiding SPPs[28]. SPPs are electromagnetic waves propagating along a metal–dielectric interface coupled to charge oscillations at the metal surface. Due to their electronic nature, the spatial wavelength of SPPs is reduced and can therefore be confined to dimensions much smaller than their angular wavelength. By placing two metal–insulator interfaces close to each other, two SPPs can couple to each other to form so-called gap or slot SPPs[28]. Such MIM slot waveguides can strongly confine and guide infrared SPPs. The insulator forming our MIM slot consists of a nonlinear optical (NLO) material. The NLO material used here is composed of organic electro-optic chromophores with a strong $\chi^{(2)}$ nonlinear response. If an electric field is applied across the NLO material, a change is induced in the material's refractive index. This way the phase of propagating SPPs along the MIM slot can be controlled with an external electrical signal. The induced phase shift $\Delta\varphi = \Delta n_{\mathrm{eff}} \times L \times 2\pi/\lambda$ is proportional to the change in effective refractive index Δn_{eff}, to device length L and to the inverse of the wavelength λ. The effective refractive index change can be expressed as[27,40].

$$\Delta n_{\mathrm{eff}} = \Gamma \frac{\Delta n_{\mathrm{mat}}}{n_{\mathrm{mat}}} n_{\mathrm{slow}} = \frac{1}{2} n_{\mathrm{mat}}^2 r_{33} \Gamma n_{\mathrm{slow}} E_{\mathrm{slot}}$$

where n_{mat} is the material refractive index, Γ is the confinement factor, n_{slot} the slow-down factor, r_{33} the nonlinear coefficient of the electro-optic material and E_{slot} the electric field in the slot. Several factors make the modulation of the SPP's phase efficient[40]. The perfect confinement in the plasmonic slot of the optical and electrical fields (see Supplementary Fig. 1b) results in their almost perfect overlap, yielding a high Γ. The bound nature of SPP fields to metals leads to the slow-down effect n_{slot} increasing the nonlinear interaction for the same optical path. In addition, the plasmonic slot allows arbitrary nonlinear materials to be chosen. Organic electro-optic chromophores have been shown to have very strong electro-optic nonlinearities r_{33}. The nanoscale dimension of the plasmonic slot results in high fields for low applied voltages. These lead to optimal nonlinear interactions and the most-efficient conversion efficiencies such that Δn_{eff} close to 0.1 can be found[40]. In addition, the subwavelength nature of the plasmonic slot enables the most-compact solution reducing the resistance-capacitance product of the device. This allows for the largest electro-optic bandwidths.

Fibre-to-device coupling. Grating couplers and Si access waveguides are used to couple the optical signal from the optical fibre to the plasmonic modulator and back to the fibre. The grating couplers couple the optical mode from the fibre to the Si waveguides. The grating couplers are formed by a periodic arrangement of Si tranches matching the wavelength to couple, for example, 1,550 nm. Subsequently, the optical energy is coupled from the Si waveguide to the plasmonic section via photonic-plasmonic converters[26,41]. The photonic-plasmonic converters consist of a tapered Si waveguide and inverted metal taper. The evanescent optical field from the Si waveguide couples on both sides to SPPs at the metal interface. At the beginning of the plasmonic slot, both SPPs couple together to form a slot SPP.

Device fabrication. Devices were fabricated on a SOI wafer with 220-nm-thick silicon layer and 3-µm-thick buried oxide. Silicon waveguides with a width of 450 nm and height of 220 nm were patterned by e-beam lithography and dry etching. The waveguides were covered with a 500 nm SiO_2 cladding. Next, the metal forming the plasmonic modulator and antenna arms were deposited by e-beam evaporation and a lift-off process. Finally, a nonlinear optical organic material composite (HD-BB-OH/YLD124) was applied by spin-coating[29]. The mesoscopic nonlinearity of the organic material was then activated by a poling procedure[31]. The total device is 900 µm in length and 350 µm wide. The plasmonic slot is 75 nm wide and 17.5 µm in length. For one set of devices, the Si substrate was thinned down to 250 µm and gold was sputtered on the back of the chip as a back reflector. Note that the device with thinned down substrate was used for the 1-m-link experiment. The additional processing on the substrate introduced some additional losses. For this reason, the 5-m-link experiment was done with a device without processing of the substrate (no back reflector).

Electro-optic characterization. Laser light at 1,550 nm was coupled to the chip by means of a grating coupler. A 60 GHz radiofrequency signal generated by a microwave synthesizer is transmitted with a horn antenna onto the chip and used to induce a modulation onto the optical carrier. The optical signal is then analysed with an optical spectrum analyser and the electro-optic response of the side bands are measured.

Fibre–wireless–fibre link demonstration. A transparent fibre–wireless–fibre link was built (see Fig. 3). First, a QPSK signal with a random bit sequence was encoded onto a 1,550 nm optical carrier (f_0) with an IQ modulator. The data signal had a symbol rate between 1 and 10 GBd and was pulse shaped with a square root raised cosine with a roll-off factor of 0.05. In the radiofrequency front-end, the data signal was combined with a second laser ($f_0 - f_{\mathrm{ref}}$), which was tuned for a wavelength offset corresponding to the radiofrequency carrier frequency, that is 60 GHz. This radiofrequency carrier was chosen due to the available equipment. Subsequently, the radiofrequency signal was generated using a high-speed (70 GHz) photodetector (Finisar XPDV3120R) with a DC responsivity of 0.6 A W^{-1}. With a delivered input optical power of 10 mW, a generated radiofrequency power of 1 mW was estimated. For comparison, typical fibre-to-the-home networks use downstream optical power levels on the order of 3 mW to support 1.2 Gbit s^{-1}. With powers on the same order of magnitude (10 mW), we achieved data rates approximately tenfold higher. To maximize the opto-electrical conversion efficiency, both laser amplitudes were kept at equal powers (see Fig. 3, left inset). The generated radiofrequency signal was then amplified by a high-power V-band amplifier (SAGE SBP-5536533022-1515-E1) providing an unsaturated gain of 30 dB, a saturation output power of 22 dBm and an electrical bandwidth of 55–65 GHz. The amplified radiofrequency signal was fed to a phased-array antenna (SENCITY Matrix, Huber+Suhner) with a gain of 38 dBi and a bandwidth of 57–66 GHz. To overcome the free-space path losses, a high-density polyethylene lens was used to focus the MMW energy onto the chip. The lens gain at 60 GHz was measured to be 18 dB. The wireless link between the transmitter and receiver was set first to 1 m. In a second step, the link was increased to 5 m. As an optical table was needed for the receiver setup, the wireless distance was limited by the distance between the optical tables in the laboratory.

The wireless signal containing the data information was then directed to the passive plasmonic mixer. An optical continuous wave signal ($f_0 - f_{\mathrm{ref}}$) was coupled into the plasmonic mixer as a new optical carrier on the receiver side. The impinging radiofrequency field modulated the laser, and light with the encoded information was coupled out of the receiver chip through the grating couplers. Subsequently, the optical signal was optically amplified in an EDFA and fed to an optical coherent receiver. The local oscillator of the coherent receiver was set to the wavelength of one of the side bands, that is, corresponding to the wavelength in the optical transmitter (f_0). Offline digital signal processing was then performed at the receiver including matched filtering, timing and carrier recovery, and linear and nonlinear equalization.

Potential of the concept to extend reach and bandwidth. Several issues can be addressed to increase the transmission link and bandwidth. So, for instance, one can improve the antenna gain in the transmitter or improve the lens gain in the receiver. The current antenna link gain of transmitter and receiver amounts to 56 dBi. Yet, 30 dB higher transmitter–receiver gains and beyond have been reported at higher frequencies[4,8,34]. Another issue to be addressed are the total losses of the chips. For the two generations of chip with and without a reflector, we measured total chip losses of 44 and 34 dB. These losses can be attributed to fibre-to-chip coupling losses on the order of 20 and 18 dB, Si waveguide propagation losses on the order of 10 and 2 dB, and losses in the active plasmonic section on the order of 14 and 12 dB, for the two chip generations, respectively. Admittedly, these losses are high and could be as low as 8 dB if fabrication was performed with state-of-the-art silicon photonics fabs. In fact, state-of-the-art optical grating couplers offered by industrial fabs guarantee coupling losses on the order of 2.5 dB per coupler[35] while losses for Si waveguides are well below 1 dB cm^{-1}. Also the losses in the active plasmonic section can be reduced. Recently, we were able to introduce a more efficient resonant plasmonic modulation scheme, where losses have been reduced to 2.5 dB (ref. [36]). Thus, by replacing the coupling schemes and implementing the most recent plasmonic modulation schemes the net-optical losses could thus be reduced by up to 26 dB, resulting in an additional 52 dB electrical power in the system. Bringing down these excess losses will allow one to leave out, for example, the electrical amplifier with a 22 dB gain in the transmitter. The additional power could also be used to map higher modulation formats such as 16-QAM onto the optical carrier[16] or for transmitting the information across longer distances. Increasing the distance from 5 m to 100 m would for instance require 25 dB out of the loss budget.

Another advantage of the scheme is the scalability to higher carrier frequencies. As the frequency response of plasmonic modulator is flat beyond 300 GHz (refs [22,25,37]), one could easily resort to a carrier frequency of around 300 GHz while preserving the current design with the 10% fractional bandwidth. This would result in an available bandwidth of 30 GHz. In a next step, one could arrange, for example, three transmitters in parallel. Parallelization is possible due to the very compact footprint of the device. Assuming three frequency bands around 300 GHz with each 30 GHz (typically this will allow the transmission of 30 GBd in each band), one could potentially transmit 3 × 60 Gbit s^{-1} of QPSK signals resulting in data rates of up to 180 Gbit s^{-1}.

In summary, the current design leaves ample margin for improvement. So there are at least 30 dB of transmitter and receiver link gain and 52 dB of link gain due to optical losses. Further, by transmitting three bands of 30 GHz at a carrier frequency of 300 GHz, the proposed concept potentially should be able to transmit 180 Gbit s^{-1} of data across a wireless distance beyond 100 m. If such a scenario were implemented, it would correspond to a bandwidth-distance product of 9 THz m.

Data availability

The data that support the plots within this paper and other findings of this study are available from the corresponding author upon reasonable request.

References

40. Haffner, C. et al. All-plasmonic Mach–Zehnder modulator enabling optical high-speed communication at the microscale. *Nat. Photon.* **9**, 525–528 (2015).

41. Tian, J., Yu, S., Yan, W. & Qiu, M. Broadband high-efficiency surface-plasmon-polariton coupler with silicon-metal interface. *Appl. Phys. Lett.* **95**, 13504 (2009).